nature communications

Article

https://doi.org/10.1038/s41467-024-53123-6

Robo-Matter towards reconfigurable multifunctional smart materials

Received: 30 April 2024

Accepted: 27 September 2024

Published online: 14 October 2024

Check for updates

Jing Wang[1,2], Gao Wang[1,2], Huaicheng Chen[1], Yanping Liu[3], Peilong Wang[1], Daming Yuan[1], Xingyu Ma[1], Xiangyu Xu[1], Zhengdong Cheng[4], Baohua Ji[5], Mingcheng Yang[2,10], Jianwei Shuai[1], Fangfu Ye[1,2,6], Jin Wang[1,7], Yang Jiao[8,9] ✉ & Liyu Liu[3] ✉

Maximizing materials utilization efficiency via enhancing their reconfigurability and multifunctionality offers a promising avenue in addressing the global challenges in sustainability. To this end, significant efforts have been made in developing reconfigurable multifunctional smart materials, which can exhibit remarkable behaviors such as morphing and self-healing. However, the difficulty in efficiently manipulating and controlling matter at the building block level with manageable cost and complexity, which is crucial to achieving superior responsiveness to environmental clues and stimuli, has significantly hindered the further development of such smart materials. Here we introduce a concept of Robo-Matter, which can be activated and controlled through external information exchange at the building block level, to enable a high-level of controllability, mutability and versatility for reconfigurable multifunctional smart materials. Using specially designed micro-robot building blocks with symmetry-breaking active motion modes, tunable anisotropic interactions, and interactive coupling with a programmable spatial-temporal dynamic light field, we demonstrate an emergent Robot-Matter duality, which enables a spectrum of desirable behaviors spanning from matter-like properties such as ultra-fast self-assembly and adaptivity, to robot-like properties including active force output, smart healing, smart morphing and infiltration. Our work demonstrates a promising direction for designing next-generation smart materials and large-scale robotic swarms.

The 1991 science fiction film Terminator 2: Judgment Day depicted an advanced robot, the T-1000, made of virtually indestructible reconfigurable material exhibiting remarkable features including rapid morphing, stiffness change, self-healing, infiltration through small structures, etc., enabled by the unique capabilities of the fundamental building blocks, including distributed information processing and exchanging, active energy conversion, as well as adaptive interactions. These characteristics collectively defined a dream material, with a ultra-high level of multifunctionality and material utilization efficiency that was impossible to make using 1990's technology. Reconfigurability and multifunctionality is a growing trend in materials, electronics components, and other important fields, which play an important role in reducing the costs of manufacturing, transportation and degradation, as well as promoting scientific and technological progress[1–4]. These advances, in turn, improve resource utilization efficiency, reduce man-made environment destruction, and promote sustainable development. But how far are we from this dream today?

The state-of-the-art smart materials are capable of actively responding to external stimuli (e.g., temperature, pressure, electric or magnetic fields, etc.)[5,6], endowing them with remarkable performance

A full list of affiliations appears at the end of the paper. ✉e-mail: yang.jiao.2@asu.edu; lyliu@cqu.edu.cn

and functionality such as adaptivity, morphing, and self-healing[7–11], which are typical features of living organisms and difficult to achieve in traditional inert materials. The responsive and programmable nature of smart materials enables a rich spectrum of applications, from sensors and actuators[12], to artificial muscles and complex biomimetic and biohybrid systems[13–15]. Smart materials based on active matter[16–20] offer a promising avenue for autonomous engineered matter[21,22]. Self-assembly (or self-organization) has been widely used in material synthesis and offers unique advantages, including high scalability and minimal control[23–25] compared to other alternatives (e.g., 3D printing[26]). However, achieving multifunctionality via self-assembly would simultaneously require information processing, energy conversion, and adjustable interaction on the building-block level, which dramatically boosts their structural complexity[27–31] and imposes significant challenges in their realizations.

On the other hand, robot swarms, i.e., systems composed of physical micro-robots (or agents) that interact among themselves and with the environment, can exhibit a rich spectrum of emergent collective behaviors, similar to living organisms[32–36]. The majority of robot swarms utilized interactions based on active signal sending and sensing, leveraging the information processing capability of individual agents[32,37]. Recently, nontrivial physical interactions (e.g., reversible binding or mechanical entanglement) are introduced that induce rich self-assembly or self-organizational behaviors in robot swarms[38–40]. For example, an amorphous assembly of entangled or cohesive robots was found to exhibit matter-like behaviors, such as state or property changes in response to demand[20,41,42]. Regulation of robot swarms via environmental cues, e.g., indirect information transduction in the stigmergic systems[43,44] has also been explored. The principles of swarm robotics[45,46] and robophysics[47] were employed to guide and analyze collective robotic behaviors, including morphogenesis[32,48], environmental adaptivity[34,49], and active target delivery[50,51]. These developments suggest that robotic materials (or intelligent matter) with distributed information exchanging and feedback capability at the building-block level, can achieve smartness that significantly extends the functionality of classical smart materials[19,52,53]. However, most existing micro-robots are very expensive to make, mainly due to the complexity of integrated information processing and computation units, significantly limiting the scale of these robotic swarms[34,37,42,54]. Simultaneously achieving tunable physical interactions and information processing capability for multifunctionality would make it even more challenging.

Here, inspired by the robotic materials, we propose an approach towards the realization of the aforementioned dream material on the macroscopic scale by introducing a Robo-Matter system, i.e., a system composed of a large number (e.g., on the order of thousands) of robotic building blocks with a minimal set of required features (discussed below) to realize desirable material functionalities, which are otherwise difficult to realize using traditional building blocks (e.g., nano-particles, and colloids[55]). As illustrated in Fig. 1, one can consider traditional matters as being made of building blocks with a low-level complexity and are only able to achieve limited functionalities. On the other hand, traditional robotic systems typically consist of highly complex agents, which are able to perform sophisticated tasks but are not cost-efficient and, thus, not scalable. We envision that the ideal Robo-Matter system shall lie between these two extremes and consist of scalable robotic agents as building blocks, achieving an optimal balance between complexity, functionality and cost performance.

To this end, we desire that a key feature of the Robo-Matter building blocks is their capability for sensing, processing, and exchanging external information, e.g., through coupling with an external environment (e.g., physical fields[56,57], whose spatial-temporal dynamics encodes the information). Accordingly, the building blocks should be able to achieve a diversity of distinguishable self-organizational collective states in response to the processed information, as well as to enhance the information exchange and spreading throughout the system and to reduce the difficulty of control via external information input. Information exchange through physical interactions of building blocks with each other and with the external environment instead of through internal digital computing components distinguishes the Robo-Matter systems from conventional robotic systems. This can be realized through the combinations of controllable active motions (e.g., symmetry-breaking polarized translations[17] or chiral rotations[58,59]) and selective physical interactions (e.g., anisotropic interactions as in Janus particles[29]). To provide a proof-of-concept of Robo-Matter in 2D, we designed and fabricated a robotic system composed of thousands of magnetic micro-robot building blocks (Magbots) and a light-emitting diode (LED) environment platform (Fig. 2a).

Importantly, as shown in the 2D Magbot system, our Robo-Matter system possesses the characteristics of Robot-Matter duality: On the one hand, the system exhibits a rich spectrum of self-organizing behaviors and transitions between the disordered and the ordered active phases in response to varying environmental driving forces or internal interactions, resembling the behaviors of active matters. On the other hand, the system exhibits robotic behaviors such as highly coordinated sequential motions of individual agents in response to specific external stimuli in order to complete complex tasks. As demonstrated below, such Robot-Matter duality enables a wide range of self-organizational behaviors and functionalities of Robo-Matter as macroscopic smart materials, including ultra-fast hierarchical self-assembly, self-adaption, active force output, smart healing, smart morphing, and infiltration, etc., some of which had been thought only possible in science fictions.

Results

Robo-Matter building blocks: Magbots

The fundamental building blocks for our 2D Robo-Matter are the Magbots (Fig. S1), which are coin-sized cylinder-shaped micro-robots (Fig. 2b, c). The Magbots are much larger than typically material building blocks (e.g., atoms or colloids), and in this sense, they realize a macroscopic-scale Robo-Matter system. As shown in Fig. 2b, c, a Magbot is composed of a vibration motor, which drives the Magbot to rotate either clockwise (CW) or counterclockwise (CCW), depending on the alignment of the brushes at the bottom (Fig. 2d). This construction leads to slight dynamic heterogeneity among the Magbots (e.g., variations in rotation speeds, Supplementary Section 1.3). Each Magbot has 6 pockets, uniformly distributed over its perimeter, which can host up to $m = 6$ freely rotating magnetic rods with tunable binding strength F_m (Figs. 2b, 3a, b, Fig. S5, and Supplementary Section 1.3.3). The Magbots are also equipped with light sensors at the bottom, allowing them to respond to a light intensity field imposed via an LED array platform. The dynamic states and trajectories of the Magbots are collected using an overhead low-latency CCD camera (Fig. 3c, d and Supplementary Section 1.2.2).

These designs not only allow massive production of the Magbots with low costs to achieve scalability (~1000 Magbots, see Fig. 2a); but also enable a combination of three key building-block features that are crucial for Robo-Matter systems (see Fig. 1 and Supplementary Section 1.1), including (i) symmetry-breaking activation (Fig. 2d, Supplementary Section 1.3.1), (ii) anisotropic tunable magnetic binding (Fig. 3a, b, Supplementary Section 1.3.3), and (iii) interactive coupling with a programmable spatial-temporal light intensity field (Fig. 3c–g, Figs. S2–S4, and Supplementary Section 1.2.2). In particular, the symmetry-breaking activation is realized through chiral rotations, which can lead to novel emergent states such as active turbulence[60], microphase separation[16,58], and topological edge flow[59]. When combined with anisotropic (binding) interactions, exotic active phases (e.g., flocking, vortices, and percolated networks[61]) can be created, providing the foundation for achieving Robo-Matter functionalities. Indeed, as demonstrated below, these features give rise to the emergence of a variety of active phases, including active (i.e.,

https://doi.org/10.1038/s41467-024-53123-6

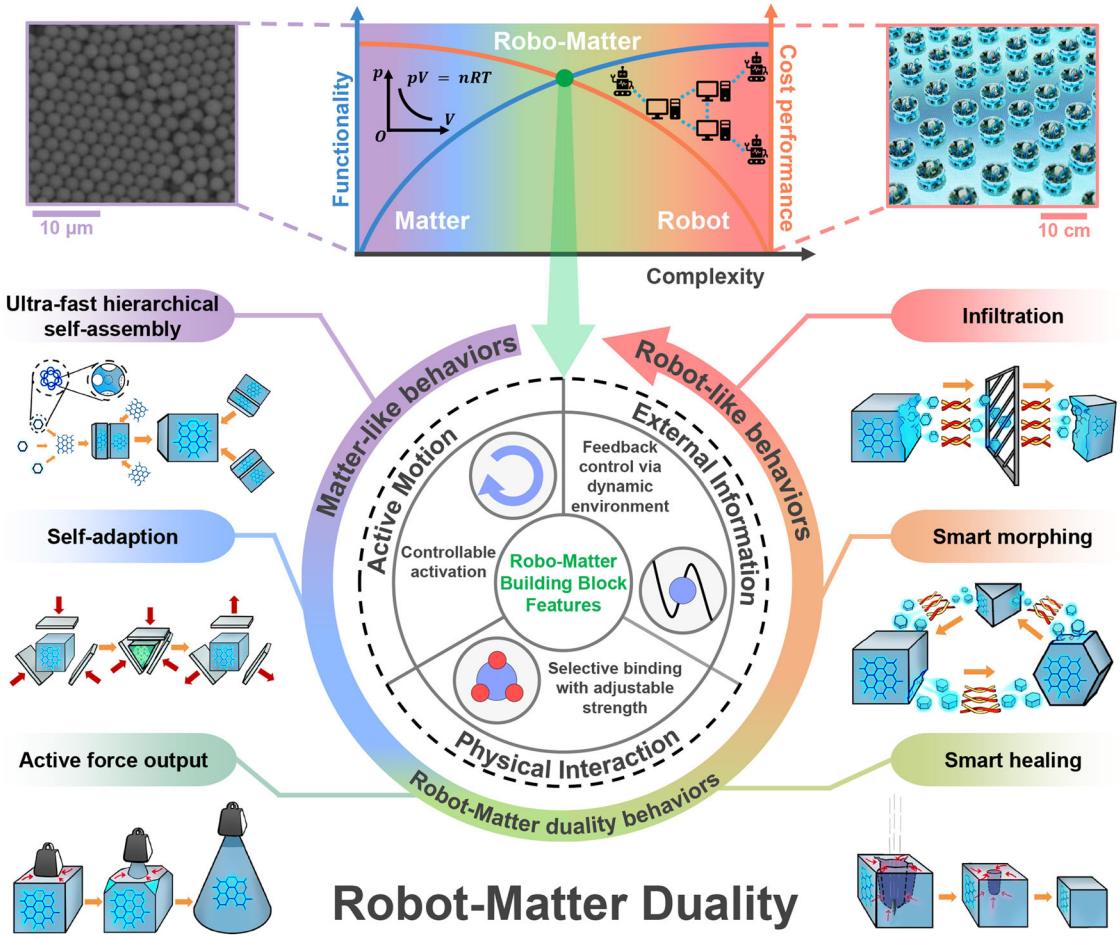

Fig. 1 | Schematic illustration of Robo-Matter system. A Robo-Matter system is one composed of a large number (e.g., on the order of thousands) of robotic building blocks with a minimal set of required features (including information sensing and processing capability, Supplementary Section 1.1) to realize desirable material functionalities and reconfigurability, which are otherwise difficult to realize using traditional building blocks (e.g., colloids). Robo-Matter system lies between the two extremes, namely, traditional matters (top left panel, reproduced from ref. 55 with permission from the Royal Society of Chemistry) and traditional robotic systems (top right panel, adapted from ref. 34 with permission) and consists of scalable robotic agents as building blocks, achieving an optimal balance between complexity, functionality and cost performance. Robo-Matter system possesses the characteristics of Robot-Matter duality, which enables a wide range of functionalities and applications of Robo-Matter as reconfigurable multi-functional smart materials, including ultra-fast hierarchical self-assembly, self-adaption, active force output, smart healing, smart morphing, and infiltration. Here we provide a proof-of-concept of Robo-Matter in two-dimension (2D) using specially designed magnetic micro-robot building blocks.

rotating) crystals[62,63] with varying structures and symmetries (see Figs. 3b, 4a).

The coupling with the light field is crucial for the presence of Robot-Matter duality. On the one hand, a homogeneous light field plays a similar role of temperature for a typical matter, where increasing light intensity I_L leads to faster rotation speeds ω_1 of the Magbots (Fig. 3f, g and Supplementary Section 1.3.1), similar to the fact that increasing temperature leads to stronger thermal motions of molecules/colloids. On the other hand, a programmed localized dynamic light field contains rich information (e.g., spot locations, impulse intensity, etc.), which can be processed by the individual or a cluster of Magbots and drive their coordinated motions, inducing diverse robotic behaviors (Fig. 3e).

Collective organizational behaviors

We systematically investigate the organizational behaviors of the Magbot systems in response to varying intensity I_L of the homogeneous light field (and thus, the activation strength $\mathcal{A}$, defined as the average kinetic energy of the Magbots), as well as varying magnetic binding force F_m (thus, the binding strength $\mathcal{E}$, defined as the average binding energy between the Magbots). We refer to the various self-organization states as phases, with the understanding that they are distinctly different from the thermodynamic phases of matter. I_L plays a similar role of temperature as in a typical matter, controlling the activation strength $\mathcal{A}$ (i.e., the rotation speed ω_1), which competes with the binding strength $\mathcal{E}$ (i.e., the magnetic binding force F_m) to determine the phase of the Magbot system. We also investigate the effects of number density ρ (i.e., number of Magbots per unit area) and boundary diameter D, which are described in Supplementary Section 3.2.

Without the loss of generality, we report the results for CW Magbots with threefold symmetric binding sites, which can form honeycomb lattice structures (Fig. 3b). Systems composed of Magbots with other types of symmetry (e.g., twofold) and chirality (i.e., CCW rotation) are reported in Supplementary Section 3.5. We employ a variety of order parameters to quantify the distinct structural, topological and dynamical features of the collective states under different $\mathcal{A}$ and $\mathcal{E}$, including the local bond-orientational order parameter ψ_6, local topological order parameter h_6, nearest-neighbor number change rate n_{nc}, and bond change rate n_{bc} (see Fig. 4b and Fig. S6 and Supplementary Section 2). ψ_6 and h_6, respectively characterizes the local geometrical and topological order in the system (Fig. S7), which can sensitively distinguish the crystalline phase from disordered

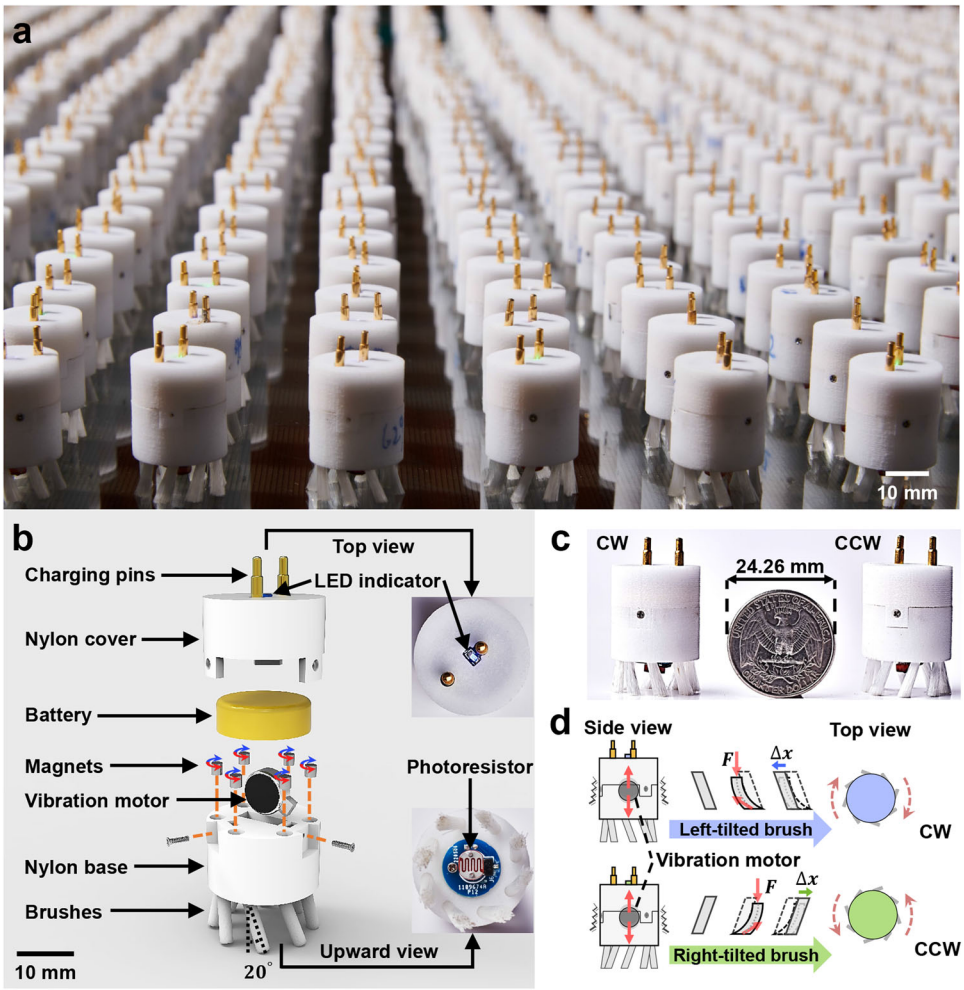

Fig. 2 | Robo-Matter building blocks: Magbots. a Swarm of ~1000 Magbots arranged in an array. **b** Schematic of the structural design of a single Magbot, which is composed of two charging pins, an LED indicator, a nylon cover, a rechargeable battery, up to six rotatable magnets, a vibration motor, a photoresistor, and a nylon base with tilted brushes (Supplementary Section 1.2.1). **c** Comparison of a US quarter coin with two Magbots of different chiralities. **d** Illustration of Magbot rotation mechanism: The vertical vibration of a Magbot driven by the internal motor repeatedly bends the titled brushes, which in turn drive the Magbot to rotate either clockwise (CW) resulted from left-tilted brushes or counterclockwise (CCW) resulted from right-tilted brushes.

phases. Both n_{nc} and n_{bc} characterize the dynamic re-organization of the Magbot swarm. n_{nc} is sensitive to significant local structural change (i.e., change of nearest neighbors); while n_{bc} is sensitive to dynamic event (e.g., bond breaking and forming, even the overall number of nearest neighbors remains the same). Based on the steady-state order parameters of a total of 171 experiments under various conditions, the thresholds of the four order parameters are determined through a K-means clustering algorithm to quantitatively distinguish different phases (see Supplementary Section 3.2).

We construct a semi-quantitative phase diagram (Fig. 4c) summarizing the self-organization states of the 3-fold Magbots, based on a synergy of comprehensive experimental and computational efforts. Due to the large $\mathcal{A}-\mathcal{E}$ parameter space, we experimentally investigate representative sub-regions of the full $\mathcal{A}-\mathcal{E}$ plane (Fig. 4c, d and Figs. S8–S11), and use simulations to complement the experiments to explore a larger parameter space to map out the approximate phase boundaries (Figs. S24–S26 and Supplementary Movie 6). The detailed data for constructing the phase diagram are provided in Supplementary Sections 3.2 and 4.2.

The Magbot system exhibits four distinct phases: an active glass-like phase, an active crystal phase (Fig. 4a), a liquid-like phase, and a gas-like phase, which are determined based on the corresponding order metric values (Fig. 4b and Supplementary Movies 1, 6). The active glass-like phase, favored by low $\mathcal{A}$ and strong $\mathcal{E}$, possesses a stable disordered network structure characterized by low ψ_6, h_6, n_{nc}, and n_{bc} values, in which the Magbots are connected by the strong magnetic binding forces. Yet, the overall structure is active, i.e., rotating clockwise, consistent with the chirality of the building blocks. The active crystal phase possesses a stable and rotating honeycomb structure, characterized by high ψ_6 and h_6, but low n_{nc} and n_{bc} values, which reflects a delicate balance between the binding forces and activation. The liquid-like phase possesses a dynamically evolving disordered network structure (low ψ_6 and h_6), i.e., the neighboring Magbots do not form stable bonds (high n_{bc}) but maintain an overall steady nearest-neighbor configuration (low n_{nc}). The liquid-like phase also contains locally closed-packed structures (i.e., Magbots with 6 closely-packed neighbors, see Fig. S11). Such structures are defects of the system, caused by the large angular momentum (high activation) of the Magbots. The gas-like phase is a highly dynamic and disordered collection of small clusters or individual Magbots, characterized by low ψ_6 and h_6, but high n_{nc} and n_{bc} values.

The transitions between different phases in response to varying $\mathcal{A}$ and $\mathcal{E}$ can be clearly seen from the phase diagram. For example, with fixing $\mathcal{E}$ (horizontal dashed lines in Fig. 4c), the system starts from an active glass-like state at low $\mathcal{A}$, where the magnetic binding force dominates over the activation. Increasing $\mathcal{A}$ is similar to

https://doi.org/10.1038/s41467-024-53123-6

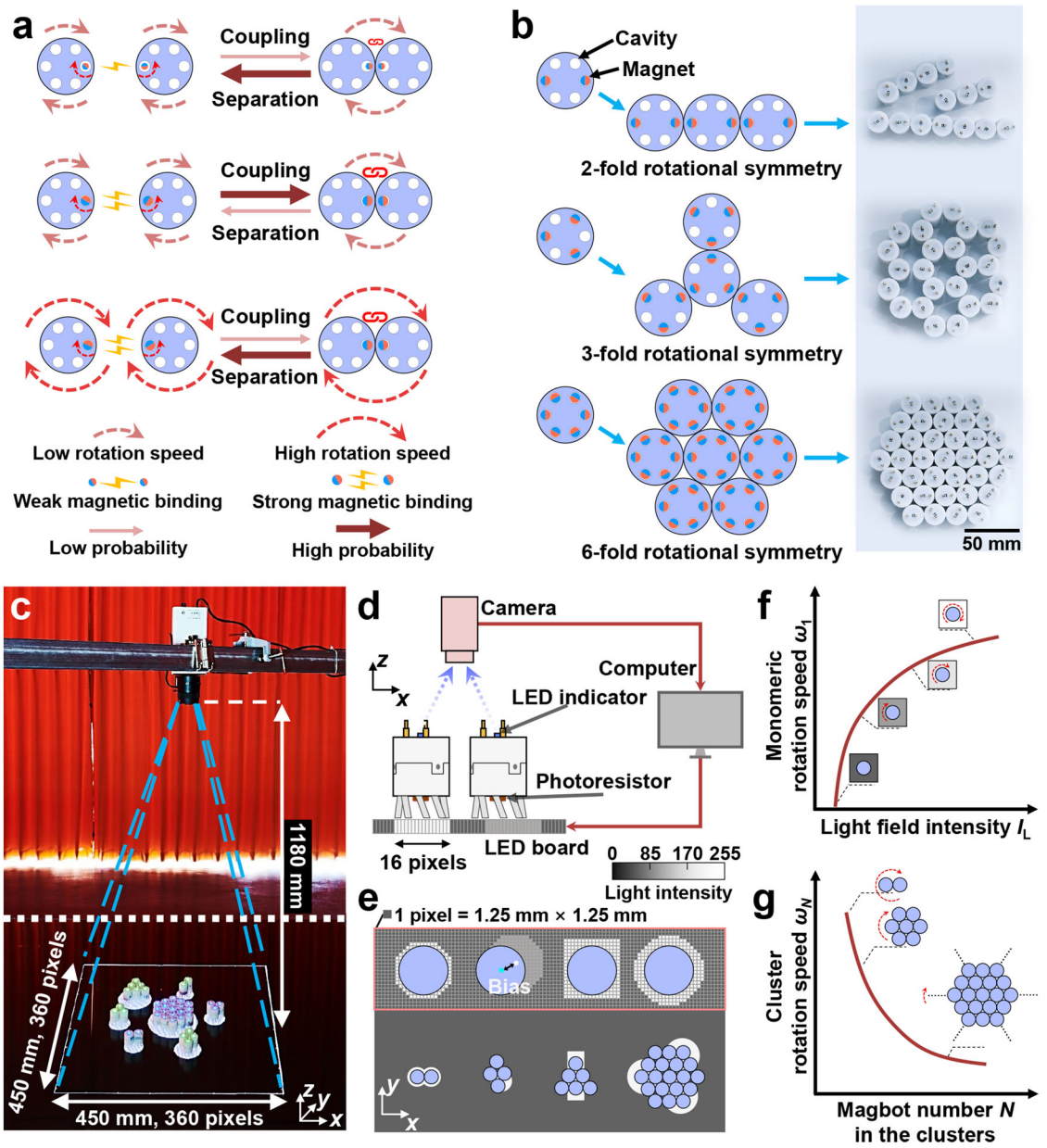

Fig. 3 | Interaction and control of Magbots. a Effect of the rotation speed and the magnetic binding strength on the coupling and the separation between Magbots. Low rotation speed and strong binding favor the coupling of Magbots, leading to a spontaneous assembly of the swarm. Increasing the rotation speed and/or decreasing the binding strength favors the separation of Magbots (Supplementary Section 1.3.3). **b** Ideal assembly structures of Magbots with different binding symmetries. Twofold, threefold, and sixfold symmetric Magbots, respectively, form chain-like, honeycomb, and close-packed hexagonal (triangular) lattices. **c** Experimental platform for the interactive light field (Supplementary Section 1.2.2). **d** Schematic illustration of the interactive light field experiments. The platform is composed of an LED light board, a CCD camera, and a computer control system. The camera captures the light signals from the LED indicators on Magbots, which are processed by the computer to capture the real-time dynamic states (position and velocity information) of the Magbots. The instantaneous state information is utilized to create a real-time complicated dynamic light field that further influences the motion of the Magbots (through their photoresistors)(Supplementary Section 3.4). **e** Examples for the interactive light field. For the case of single Magbots, the intensity, relative position, shape, and size of the interactive light spots all can change in real time based on the instantaneous state of individual Magbots or their clusters, according to a given algorithm. **f** The rotation speed of individual Magbots increases with increasing light field intensity (Supplementary Section 1.3.1). **g** The rotation speed of Magbot clusters decreases with increasing Magbot number in the clusters (Supplementary Section 1.3.1).

increasing temperature in traditional materials, allowing the system to kinetically relax to the more stable active crystal phase, which subsequently melts into a liquid-like phase. Further increasing $\mathcal{A}$ leads to a transition from the liquid-like phase to the gas-like phase, in which the high activation (i.e., high rotation speed) of the Magbots dominates over the binding forces. Increasing $\mathcal{E}$ requires larger activation to balance or destroy the binding, which gives rise to the overall positive slopes of the phase boundaries. At very low $\mathcal{E}$ and $\mathcal{A}$, the system directly undergoes a transition from the active glass-like phase to the liquid-like phase with increasing $\mathcal{A}$ or decreasing $\mathcal{E}$ (Fig. S25). In the case of fixing $\mathcal{A}$ (vertical dashed lines in Fig. 4c), the system starts from the highly dynamic and unstable gas-like phase at low $\mathcal{E}$. Increasing $\mathcal{E}$ leads to a series of transitions from the gas-like phase to the liquid-like phase, then to the active crystal phase, and eventually to the active glass-like phase. These organizational behaviors are crucial to the subsequent self-adaptive characteristics and

https://doi.org/10.1038/s41467-024-53123-6

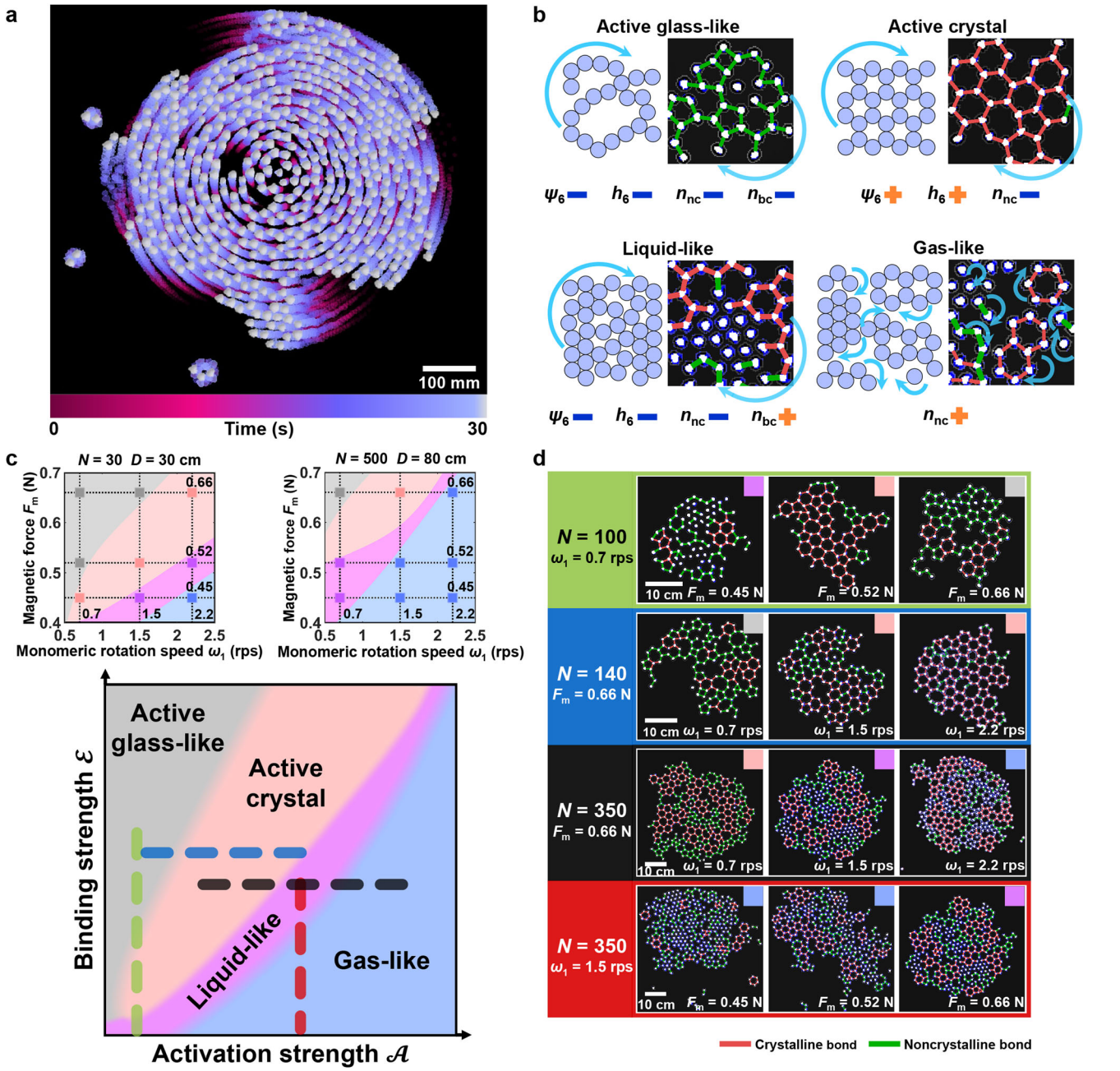

Fig. 4 | Phase diagram of Robo-Matter. Without loss of generality, the representative organizational behaviors of threefold symmetric Magbots with clockwise rotation are reported here. **a** Magbots assembled into a crystal performing an overall clockwise rotation. **b** Distinct organizational behaviors (i.e., phases) of the Magbot swarm (Supplementary Movie 1). Each panel shows a schematic of the phase (left) and an experimental snapshot (right). The blue arrows indicate clockwise rotations. The active glass-like phase corresponds to a stable and disordered network of Magbots containing large cavities and broken chains, with clockwise rotation. The active crystal phase possesses a stable and clockwise-rotating honeycomb structure. The liquid-like phase possesses a disordered and clockwise-rotating network structure, which undergoes constant dynamic re-organization. The gas-like phase contains many rotating small clusters or individual Magbots, and thus is highly dynamic and disordered. **c** A semi-quantitative phase diagram of the Magbot swarm (bottom) informed by experimental phase diagrams (two examples with different Magbot number N and boundary diameter D are shown in the top panel, Supplementary Section 3.2) and simulations (Supplementary Section 4.2) with color code: gray (active glass-like), pink (active crystal), purple (liquid-like), and blue (gas-like). **d** Representative experimental snapshots of distinct phases along the color-coded dashed lines in the semi-quantitative phase diagram. In the snapshots, the red lines highlight the bonds in locally ordered regions, and the green lines correspond to bonds in locally disordered regions.

function engineering of Robo-Matter as reconfigurable multifunctional smart materials.

Robo-Matter as a reconfigurable multifunctional smart material

The various active phases of the Magbot-based Robo-Matter system enable us to engineer many material properties, including self-correction (Fig. 5) and environmental responsiveness (Fig. 6). For example, the symmetry-breaking activation (CW or CCW rotations) of the individual building blocks is preserved when they bind together to form larger-scale structures (e.g., clusters or rings of Magbots), which are also rotating. The rotations of these larger-scale structures then facilitate their assembly into even larger structures (Fig. 5a, Fig. S12, and Supplementary Movie 2). This mechanism leads to an ultra-fast hierarchical self-assembly of Robo-Matter, characterized by the large

https://doi.org/10.1038/s41467-024-53123-6

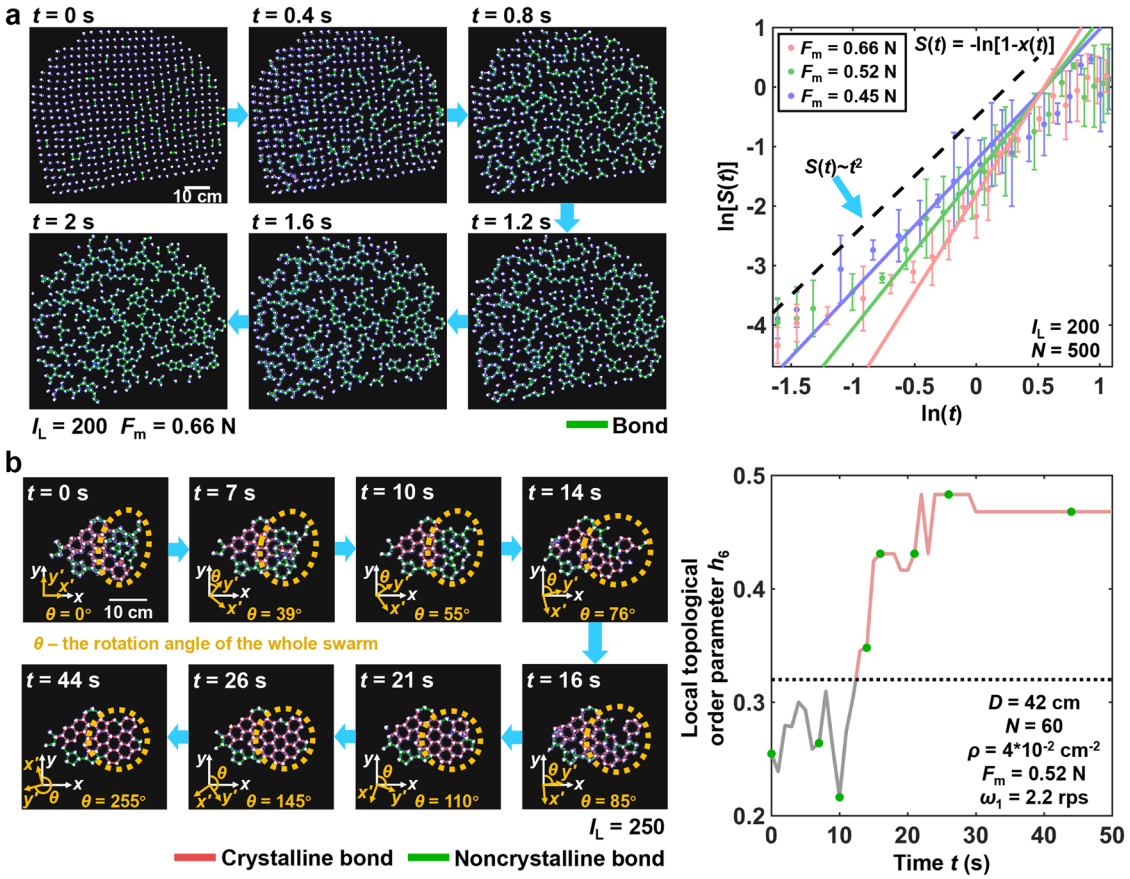

Fig. 5 | Self-assembly of Robo-Matter. a Ultra-fast hierarchical self-assembly. Left panels show the snapshots of the assembly process of 500 Magbots with 0.66 N magnets in a homogeneous light field with an intensity $I_L = 200$ a.u., where the green lines highlight the bonds between Magbots (Supplementary Movie 2). The right panel shows the dynamic function $S(t) = -[1 - x(t)]$ in logarithmic scales for varying magnetic binding strength, where $x(t)$ is the fraction of Magbots in a largest assembled cluster at time t. The Avrami index α associated with $S(t) \sim t^{\alpha}$ increases with increasing magnetic binding strength and achieves the maximum $\alpha \approx 3.3$ for the strongest magnets (0.66 N). The error bars represent the standard deviations, and the experiments have been performed for six times for each magnetic binding strength. **b** Structural self-correction (left panels) in which a disordered local region (indicated by the yellow dotted circle) broke down and reassembled into a honeycomb structure (Supplementary Movie 2). The corresponding evolution of the local topological order parameter h_6 is shown in the right panel. The red and green lines in the snapshots shown in (**b**) respectively highlight the bonds in locally ordered and disordered regions. The horizontal dotted lines in the data graphs represent the thresholds of the corresponding order parameters.

Avrami index $\alpha \in (2.2, 3.3)$ for varying magnetic binding strengths (Supplementary Section 3.3.1), which is associated with the dynamic function $S(t) \sim t^{\alpha}$. Specifically, $S(t)$ is defined through the Avrami equation[64]: $x(t) = 1 - \exp[-S(t)]$, where $x(t)$ is the fraction of Magbots in largest assembled cluster at time t. This is a contrast to the diffusion-controlled self-assembly of traditional matters (characterized by $\alpha = 2$ in 2D), where nucleated clusters are essentially immobile and their growth mainly depends on the slowly diffusive transport of individual building blocks. In addition, the Robo-Matter system also exhibits robust self-correction behaviors in the self-assembly process, where a disordered region in the active crystal phase (i.e., structural defect) can spontaneously re-organize into the crystalline honeycomb structure (Fig. 5b, Fig. S13, Supplementary Movie 2 and Supplementary Section 3.3.2). This is enabled by the active nature of the Robo-Matter phases, i.e., the rotations of the overall assembled structures and individual Magbots can easily break the relatively weak magnetic bonds in the disordered region and allow re-organization and subsequent formation of strong bonds between the Magbots.

The Robo-Matter system also demonstrates adaptivity in response to different types of external stimuli. As shown in Fig. 6a, Figs. S14, S15, S27, and Supplementary Movies 2, 6, under an isovolumetric compression, the system undergoes a transition from an initial active crystal phase (on an open honeycomb lattice) to a denser, disordered gas-like phase, in order to accommodate the geometrical confinement along the horizontal direction (Supplementary Section 3.3.3). Up on a reverse isovolumetric expansion, the active crystal phase is restored. These properties are crucial for shape-memory and morphing material applications. On the other hand, as shown in Fig. 6b, Figs. S16, S28, and Supplementary Movies 2, 6, a disordered glassy structure can rapidly re-organize and self-optimize into an active crystal in response to a sharp increase of the light field intensity (Supplementary Section 3.3.4). This behavior is similar to the structural relaxation of a non-equilibrium glass state to an equilibrium crystalline state at elevated temperature, albeit the process is much faster in Robo-Matter. The resulting active crystal phase remains ultra-stable at low activation (i.e., low light intensity), providing a convenient pathway for realizing crystalline Robo-Matter states. The capabilities for ultra-fast hierarchical self-assembly, structural self-correction, and adaptive responsiveness to external stimuli demonstrate that the Robo-Matter system would be a candidate for reconfigurable multifunctional smart material.

Diverse functionalities enabled by Robot-Matter duality

The Robot-Matter duality is a defining feature of Robo-Matter. In the previous sections, we have mainly focused on the matter aspect of the system, where the light field is kept homogeneous with varying

https://doi.org/10.1038/s41467-024-53123-6

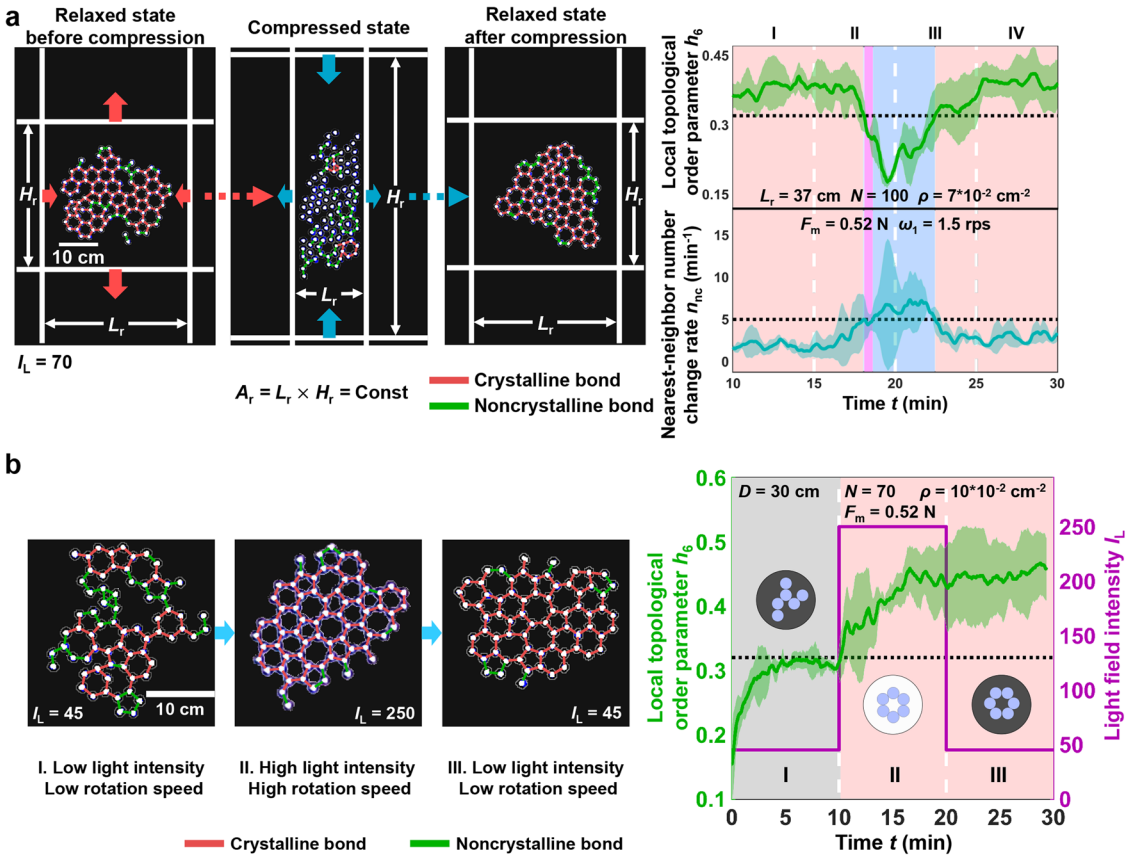

Fig. 6 | Environmental responsiveness of Robo-Matter. a Adaptivity of Robo-Matter in response to external stimuli. Left panels show the snapshots of a reversible active crystal to disordered gas-like phase transition induced by an isovolumetric compression and decompression cycle (Supplementary Movie 2). The right panel shows the evolution of h_6 and the nearest-neighbor number change rate n_{nc} during the process. The stages I, II, III, and IV, respectively corresponds to the relaxed state before compression, the compression process, the decompression process, and the relaxed state after compression. **b** Structural self-optimization of Robo-Matter in a rapidly changing environmental field. Left panels show the snapshots of a rapid re-organization and self-optimization of an active glass-like phase with disordered structures into an ultra-stable active crystal phase in response to a sharp increase-decrease of the light intensity (Supplementary Movie 2). The right panel shows the evolution of h_6 in response to a square impulse of light intensity profile. The red and green lines in the snapshots respectively highlight the bonds in locally ordered and disordered regions. The horizontal dotted lines in the data graphs represent the thresholds of the corresponding order parameters. The shaded regions in the data graphs represent the standard deviations, and the background colors indicate different phases. All the repeated experiments have been performed three times.

intensity, playing a similar role as a uniform temperature field. On the other hand, a spatial-temporal dynamic light field encodes rich information, which can be sensed and processed by the Magbot building blocks. The motions of Magbots, in turn, influence the dynamics of the light field, enabled by high-precision individual Magbot tracking and a programmable LED platform (Supplementary Section 3.4). In this context, stronger information exchange can involve, e.g., a complex dynamic pattern of localized light spots and an increasing number of independent Magbots and Magbot clusters. This interactive information exchange mechanism between Magbots and light field activates the diverse robotic behaviors of the system (e.g., complex and highly coordinated motions of individual or small clusters of Magbots), which in turn enables a wide spectrum of robot-like functionalities not present in traditional smart materials and provides a proof-of-concept of reconfigurable multifunctional smart materials.

As shown in Fig. 7a, the combinations of the basic features of the Magbot building blocks, such as magnetic binding and unbinding via magnet replacement, symmetry-breaking rotation, and information sensing and processing, lead to several fundamental responsive behaviors of groups of Magbots, including coupling and decoupling as well as asymmetric rotation of Magbot clusters. These group behaviors, in turn, contribute to higher-level functions of the Robo-Matter, such as coordinated migration (Fig. S17 and Supplementary Section 3.4.1), assembly, and disassembly that are essential to achieving desirable robotic behaviors. Fig. 7b–g demonstrate a rich spectrum of robot-like behaviors and functionalities of the Robo-Matter system (Supplementary Movie 3). These examples are organized according to the minimal number Λ of the independent Magbot clusters involved in the process and indicated by the gray-yellow color bar in the upper-right corner of each figure. A small Λ (gray bar) indicates strong matter-like behaviors (e.g., Fig. 7b) and a big Λ (yellow bar) such as in the case of infiltration (Fig. 7f) indicates strong robot-like behaviors.

Figure 7b demonstrates the capability of active force generation and output by a rectangle-shaped crystal of sixfold Magbots. The crystal as a whole is driven by a programmed dynamic light field to generate specific rotations and exert active forces on the target objects (e.g., a ping-pang ball in our experiments), in order to generate desirable locomotion of the objects, implying that the Robo-Matter could be utilized to carry cargoes to destinations. Fig. 7c shows an example of coordinated internal motion, where two smaller blocks (green) of a large-scale assembly of sixfold Magbots are weakly bound to the central block (blue), while the binding between the Magbots within each block is strong. Driven by the automatic interactive dynamic light field (Fig. S18 and Supplementary Section 3.4.2), the two smaller blocks undergo cyclic CCW rotations around the central block, during which the centers of the three blocks remain collinear. This case

https://doi.org/10.1038/s41467-024-53123-6

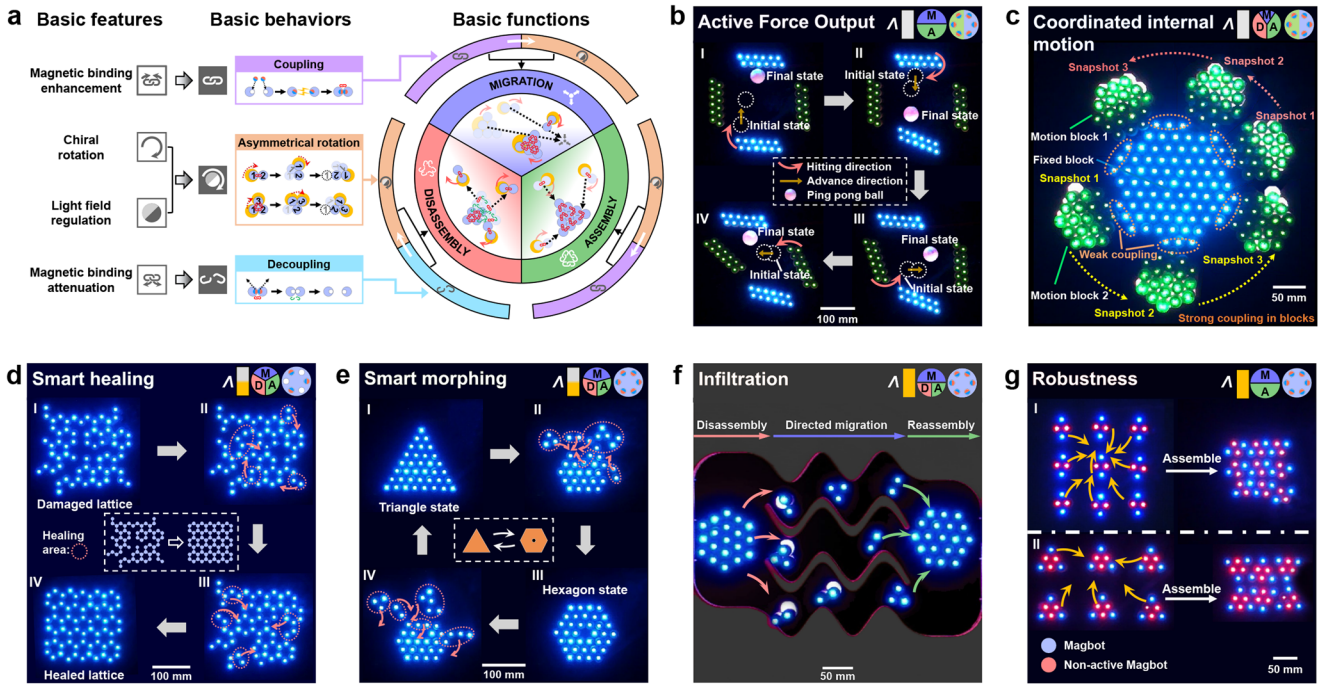

Fig. 7 | Various functionalities enabled by Robot-Matter duality. a Schematic illustration of the basic functions of Robo-Matter. These basic functions are based on several fundamental responsive behaviors of groups of Magbots, which in turn are enabled by combinations of basic features of the Magbot building blocks. **b**–**g** Demonstrates several robotic behaviors of the Robo-Matter system, leveraging the Robot-Matter duality. In the upper-right corner of each figure, the color bar qualitatively indicates the level of matter-like (gray) and robot-like behaviors (yellow); the pie chart reflects the portion of the basic functions, including directed migration (blue), assembly (green), and disassembly (red); the six-hole disk indicates the type of Magbots. Supplementary Movie 3 illustrates these robotic behaviors. **b** Active force output: a crystalline assembly of sixfold Magbots can take specific rotary motions (as indicated by the red arrows) in response to a dynamic light field, and actively exert significant forces on the target objects, causing the target objects to make desirable locomotion (as indicated by the yellow arrows). **c** Coordinated internal motion: Two smaller blocks (green) of a large-scale assembly of sixfold Magbots that are weakly bound to the central block (blue) undergo cyclic counterclockwise rotations around the central block, driven by an automatic interactive dynamic light field. **d** Smart healing: The disassembled Magbots migrate to the appropriate positions guided by interactive localized light information, and re-assemble to the main part again to form a defect-free crystalline structure. **e** Smart morphing: A portion of the peripheral regions of the system can be shaped to various conformations through the disassembly-migration-reassembly process. **f** Infiltration: A large Magbot assembly can get through narrow and complex channels by completely disassembling to minimal controllable units and directionally migrating through the channels via the automatic light field, and then restoring the original shape by reassembling at the other end of the channels. **g** Robustness: Proper assembly modes (e.g., the type I and type II as shown) can make separated, and small Magbot clusters composed of normal Magbots and non-active Magbots (red) still have the ability to directionally migrate (indicated by the yellow arrows).

demonstrates that a Magbot assembly with heterogeneous coupling could mimic driving units in some machinery, such as pumps and transmissions. The above two examples, both showing strong matter-like behaviors, imply the potential applications of the Robo-Matter system in delicate transportation and delivery[36,50].

Figure 7d shows an example of the smart healing process of a honeycomb crystal of threefold Magbots, in which the system exhibits mixed matter-like and robot-like behaviors. Specifically, the magnetic binding strength is decreased in the damaged regions to allow several specific Magbot clusters disassembled from the majority of the system. The disassembled building blocks are subsequently transported to the desirable locations via directed migration induced by the dynamic light field, which are then reassembled by increasing the binding strength to form a honeycomb crystal. Compared to the aforementioned self-healing process, which is driven by a homogeneous light field (see Figs. 5b, 6a), the smart healing process is much more precise and efficient, enabled by the interactive information exchange between the Robo-Matter system and the dynamic light field, making the Robo-Matter a plausible candidate as protective materials which often encounter damage from the external impact or collision. Figure 7e shows an example of the active morphing of a Robo-Matter, from a triangle-shaped crystal of sixfold Magbots to a hexagon-shaped crystal, involving coordinated motions of the peripheral Magbots. During the process, a portion of the peripheral regions of the original triangle-shaped crystal (i.e., the corners) was disassembled and transformed. Therefore, smart morphing is also a mixture of matter-like and robot-like behaviors and is distinct from the responsive morphing process of the existing smart materials[65], which generally does not involve the structural re-organization of the fundamental building blocks. Notably, this morphing capability is a direct manifestation of the high reconfigurability of the Robo-Matter, suggesting it could be used to make tools with multiple stable shapes for different purposes.

Figure 7f demonstrates the capability of an active crystal of sixfold Magbots in infiltrating through a complex barrier landscape via a disassembly-migration-assembly process (Supplementary Section 3.4.2). The system exhibits strong robotic characteristics during the process, with the entire crystal breaking down to minimal controllable units to perform specific migration tasks driven by an interactive dynamic light intensity field composed of a sequence of localized impulses dynamically tracking the disassembled building blocks (Figs. S19, S20), and re-assemble to reconstruct the original crystal. This function could facilitate bulk Robo-Matter to infiltrate through porous barriers to reach its final destination. Last but not least, Fig. 7g demonstrates the robustness of the Robo-Matter system. For example, even if a certain number of the Magbots are non-functional or inactive (e.g., running out of battery), successful assembly involving small Magbot clusters (e.g., the type I and type II as shown), composed of both functional and non-active Magbots (red),

can still be achieved, by driving the functional Magbots (indicated by the yellow arrows) via the interactive localized light field. This robustness could increase the lifespan of the Robo-Matter when used in a harsh or energy-deficient environment.

Leveraging the aforementioned robotic behaviors, Robo-Matter can also be utilized to search and carry a cargo out of a complex-shaped narrow channel and form a protective shell around the cargo, as demonstrated here on a 2D plane (Fig. S21, Supplementary Movie 3, and Supplementary Section 3.4.3). Notably, active force output, smart morphing, infiltration and robustness functions all have been used in this application. Based on this principle, in future, 3D micro-scale Robo-Matter may enter the human body as a capsule and disassemble into smaller clusters upon encountering narrow channels such as intestines and blood vessels. These smaller clusters would then be able to push and encapsulate targeted foreign objects upon contact. This case illustrates the advantage and application potential of Robo-Matter in a more realistic situation.

Discussion

We have demonstrated a realization of Robo-Matter in 2D using symmetry-breaking Magbot building blocks capable of exchanging information with a programmable interactive dynamic light field, as a proof-of-concept for an economical and promising form of reconfigurable multifunctional smart materials. This macroscopic-scale model Robo-Matter system possesses the property of Robot-Matter duality, enabling a wide range of functionalities and applications, which are beyond the capability of both traditional inert and active materials. We showed how to achieve various characteristics and functions based on the different collective states, which illustrated that distributed information interaction is a key factor in the design and realization of next-generation smart materials. Although our demonstrations are mainly based on threefold and sixfold Magbots, we have also investigated other anisotropic configuration of magnetic binding sites, which are discussed in Supplementary Section 3.5. For example, a polarized Magbot with two binding sites can form stable chain-like structures (Fig. S22), which can be used for building blocks of robotic polymers (Supplementary Movie 4). In addition, we have investigated the effects of mixing chirality in systems consisting of both CW and CCW Magbots (Fig. S23), which are discussed in detail in Supplementary Section 3.6 and shown in Supplementary Movie 5.

Many collective Robo-Matter behaviors, such as state transition[34], phase separation[58], and morphing[32], were also observed in previously studied systems. These similarities make the insights gained from Robo-Matter transformative, potentially applicable in a broad spectrum of active systems. On the other hand, the Robo-Matter system distinguishes itself via specific microscopic mechanisms. For example, the stable and tunable soft bonds between the Magbots can support stable structures with exotic mechanical properties, compared to the loose structures obtained in many active systems. Furthermore, the active nature of the collective Robo-Matter states, which brings the self-assembly properties and environmental responsiveness, is another key distinguishing features of the system. Although distributed environmental cues are also used in stigmergic robot swarms[43,44], our system unitizes feedback environmental interactions based on the instantaneous dynamical state of Robo-Matter, rather than passive media depending on existing environmental constructions.

While our Magbot system provides a demonstration of the Robo-Matter concept on a 2D plane, realizing 3D Robo-Matter is still a challenging task and exciting research direction. For example, the handedness of a 3D object depends on viewing angle[66], and the relationship between structural chirality and chiral behavior becomes fuzzy[67], and thus, the definition and realization of symmetry-breaking activation in 3D are much more difficult than in 2D. On the other hand, many achievements have been made in 3D self-assembly[40,68–70] which could inspire our future work. To deal with the influence of gravity in 3D motion, an efficient and precise driving structure could be used to replace the current vibration-driven motion mode. Magnetic soft connections, benefiting from the ease of manipulation, flexibility, minimal control, and low complexity, is still a highly suitable choice for reconfigurable 3D structures. Last but not least, when the environmental field control is applied in 3D self-assembly, the external electromagnetic field with strong penetration may be a better choice than the light field used in the Magbot system. The integration and realization of these features in the building blocks of the 3D Robo-Matter still require significant technical innovations.

The rich spectrum of properties, rooted in the diverse collective Robo-Matter phases and spanning from matter-like to robot-like ones, also enables a wide range of promising potential applications of Robo-Matter. For example, the liquid-like Robo-Matter can easily go over an obstacle, get through narrow channels, or dynamically adjust the internal structure, enabling the system to overcome complex terrains to reach the destinations and switch or retain its own shapes and functions. The active crystal Robo-Matter could carry cargoes, resist external impact, or generate active forces, thus having the potential in distributed construction and protection. Once realized in 3D, the controllable transition between liquid-like and active crystal states via external cues would enable the Robo-Matter system to perform a variety of tasks in complex environments. For example, carefully designed macro-scale Robo-Matter (each unit ~0.1 m) could infiltrate into the ruins to rescue the victims and aid with post-disaster reconstruction, or explore underground caves to collect samples. Microscopic Robo-Matter (each unit ~1 μm) could help deliver targeted drugs, clear clogged blood vessels, or hunt down and kill targeted malignant cells or tissues in vivo.

Our work also has important implications and provides technical insights into the design and realization of the next-generation autonomous engineered matter with high reconfigurability, multifunctionality, and robustness. On one hand, we demonstrate the feasibility of using micro-robots as building blocks for scalable self-assembly of reconfigurable multifunctional smart materials. On the other hand, the Magbot design and fabrication also illustrate the desirable features for material building blocks (e.g., information processing capability, active energy conversion, and adjustable interaction) to achieve high reconfigurability, multifunctionality, and smartness, which would inspire new building-block design and associated technology development.

Methods

Fabrication and control of Magbots

The main supporting structures of a Magbot are 3D-printed parts made of nylon material. The lower structure is implanted with brushes made of DuPont material with an inclined angle $\Theta = 20^{\circ}$ to achieve chiral rotation behaviors. The inclination direction of the brushes determines the rotation direction of the Magbot. There are 6 empty slots for placing cylindrical magnets in the lower structure. Magnets with different heights and magnetic properties can be placed in Magbots according to experimental requirements. The entire structure is secured together into a tightly fastened entity by screws. The electronic circuitry of a Magbot consists of a rechargeable lithium button battery, a vibration motor, a photosensitive resistor, a transistor, an LED indicator, two charging pins, and several connecting soft wires. The circuit mechanism of a Magbot is as follows: the bottom photoresistor senses the ambient light intensity and changes the electric current at the base of the triode, thereby changing the power obtained by the vibration motor at the collector terminal of the triode. The higher the light intensity is, the higher the vibration frequency of the vibration motor becomes. The bottom brushes positively convert the vibration frequency of the motor into the rotation speed of the Magbot. The base of the triode is connected to a tiny LED indicator, which is placed on the top of the Magbot. Its brightness is positively

correlated with the base electric current. The clockwise Magbot is equipped with a blue LED, and the counterclockwise Magbot is equipped with a green LED. When a Magbot runs out of battery power, the battery of the Magbot can be easily charged through the two top vertical metal pins by connecting the positive and negative terminals of the battery, respectively, to an external power supply.

The dynamic and high spatiotemporal-resolution light field is composed of an LED panel with a size of 2250 mm × 2250 mm and a pixel resolution of 1800 pixels × 1800 pixels. The spacing between the LED lamp beads on the panel is 1.25 mm, both horizontally and vertically. Each LED lamp bead can independently emit light with an adjustable intensity (256 optional levels) respectively in red, green, and blue. A custom-developed screen control program enables pixel-level control of the light environment, thus achieving the presentation of various specific light patterns below the designated Magbots. The camera placed above the LED platform captures the LED light signals from the top center of Magbots, facilitating a comprehensive monitoring of all Magbots' locations. The computer located adjacent to the platform processes the images captured by the camera in real-time and generates the light patterns displayed on the LED platform according to predefined rules, achieving a rapid refresh of the LED plane. The light patterns displayed on the LED platform are sensed by photosensitive resistors at the bottom of the Magbots, thereby regulating the Magbots' motion behaviors. Consequently, the system consisting of the LED indicators on the Magbots' top, the camera, the computer processor, the light field platform, and the Magbots' photosensitive resistors forms a closed-loop feedback system, enabling the precise control and manipulation of the collective dynamics of the Magbot swarm on the platform.

Image processing

The instantaneous position information of every Magbot can be recorded by the real-time pictures from the overhead camera, which are composed of the light-spot signals from the LED indicators on the top of Magbots and the light field as a background. Combining spatial filtering, image sharpening, brightness adjustment and morphologic processing, the homogeneity and contrast of the light-spot signals can be significantly enhanced. Then the information of each light spot can be independently extracted based on the intensity and morphological features. Finally, the information of a Magbot at different time points can be concatenated into a sequence through a tracking algorithm based on the distances and historical relative position relationships.

Self-assembly experiment

Before each experiment, the Magbots had been placed on the platform in an arrangement which is a hybrid of a square matrix and random noise to make the results of different experiments comparable. Because of the starting intensity and heterogeneity, the intensity of the homogeneous light field jumped from 0 to 200 a.u. at the beginning of each experiment and kept for 3 s before jumping to the set value. This short starting stage advanced slightly the whole evolution but had almost no influence upon the final swarm state of the Magbots after a long-term evolution. Combining the center-to-center distance information calculated from the position sequences and the neighbor boundary threshold (23 mm used here), the nearest-neighbor relationships between Magbots at different time points can be determined. Then a bond is identified if two Magbots remain as neighbors over a certain period of time (one second used here). The bonding configuration of a Magbot would be corrected according to the center-to-center distance information if the bond number exceeds the number of magnetic binding sites. Next, structural and dynamical order parameters are calculated to quantify the collective organizational behaviors of Magbot swarms. The final swarm state of each experiment can be characterized by the time averages of the order parameters of the second half of the experiment. Based on the final-state order parameters of all the experiments under various conditions, the categorization thresholds of the order parameters are determined through a K-means clustering algorithm.

Compression experiment

A homemade automatic device, which is composed of four mobile hard boundaries driven by four separate programmable drive motors, was used in this work to achieve various boundary changes, such as isotropic compression-decompression and isovolumetric compression-decompression. For the isovolumetric compression experiments, in the first 15 min, the Magbot swarms can freely self-assemble into the active crystal phases. Then, the two vertical boundaries symmetrically move toward the center for 5 min, which makes the length L_r of the short sides decrease at a constant rate of 0.74 mm/s until it reaches 40% of the initial length. At the same time, the two horizontal boundaries symmetrically move outward to change the length H_r of the long sides, which makes the area $A_r = L_r \times H_r$ enclosed by the boundaries keep constant. Next, a reverse isovolumetric expansion lasts for another 5 minutes until the boundaries return to their original positions.

Robotic behavior experiment

The robotic behaviors of the Magbot system are made up of three basic swarm behaviors, i.e., assembly, disassembly, and directed migration, in various combination ways. In these basic behaviors, the interactive light field serves different purposes. For swarm assembly, the dispersed swarms gather together driven by the interactive light field and the relative positions between Magbots need delicate adjustments through the interactive light field before the magnetic coupling, hence the change modes of the light field patterns are complex and highly dependent on the specific spatial distributions of Magbots. For swarm disassembly, the small clusters are driven in all directions by the interactive light field after magnetic decoupling, hence the patterns of the light field are highly arbitrary. For directed migration, the swarms are driven to a fixed position or along a fixed direction through the interactive light field, hence it can be achieved according to some simple, fixed and unified motion rules. Based on these features of the basic behaviors, in the experiments, the assembly and disassembly were controlled through the manual interactive light field with a self-made man-machine interactive system, while the long-distance directed migration was controlled through the automatic interactive light field. To drive Magbot swarms to take specific actions, one of the key points is the selection of activated Magbots. In an open space, the directed migration to a fixed position can be automatically driven by putting the light spots directly below the Magbots, which are the farthest ones from the reference target position. In the coordinated internal motion, the outermost Magbots are automatically driven to make the counterclockwise blocks move around the central fixed block. Finally, the directed migration in channels is dependent on the reference positions related to the orientations of the target edges, which are based on the chirality and migration direction of the Magbots. Using the maximum distance principle, the long-distance infiltration in channels is achieved by an automatically interactive light field. In this process, after defining automatic and manual regions and setting target edges, coordinates of all Magbots will be obtained, automatic blocks will be identified, corresponding reference points and activation points will be calculated, and the light spots will be placed at the activation points.

Data availability

All data needed to evaluate the conclusions in this paper are present either in the main text or in the supplementary materials. Raw data generated in this study have been deposited in Zenodo[71].

Code availability

Computer codes about automatic control and simulation of the Magbot system are available online at Zenodo[71].

References

1. Lyke, J. C., Christodoulou, C. G., Vera, G. A. & Edwards, A. H. An introduction to reconfigurable systems. *Proc. IEEE* **103**, 291–317 (2015).
2. Haghpanah, B., Salari-Sharif, L., Pourrajab, P., Hopkins, J. & Valdevit, L. Multistable shape-reconfigurable architected materials. *Adv. Mater.* **28**, 7915–7920 (2016).
3. Webber, M. J. & Tibbitt, M. W. Dynamic and reconfigurable materials from reversible network interactions. *Nat. Rev. Mater.* **7**, 541–556 (2022).
4. Oliveri, G., Werner, D. H. & Massa, A. Reconfigurable electromagnetics through metamaterials?a review. *Proc. IEEE* **103**, 1034–1056 (2015).
5. Mahapatra, S. D. et al. Piezoelectric materials for energy harvesting and sensing applications: Roadmap for future smart materials. *Adv. Sci.* **8**, 2100864 (2021).
6. Yang, P. et al. Stimuli-responsive polydopamine-based smart materials. *Chem. Soc. Rev.* **50**, 8319–8343 (2021).
7. Rodriguez-Hernandez, J., Chécot, F., Gnanou, Y. & Lecommandoux, S. Toward 'smart'nano-objects by self-assembly of block copolymers in solution. *Prog. Polym. Sci.* **30**, 691–724 (2005).
8. Jochum, F. D. & Theato, P. Temperature-and light-responsive smart polymer materials. *Chem. Soc. Rev.* **42**, 7468–7483 (2013).
9. Lu, Y., Aimetti, A. A., Langer, R. & Gu, Z. Bioresponsive materials. *Nat. Rev. Mater.* **2**, 1–17 (2016).
10. Niu, W. et al. Photonic vitrimer elastomer with self-healing, high toughness, mechanochromism, and excellent durability based on dynamic covalent bond. *Adv. Funct. Mater.* **31**, 2009017 (2021).
11. Wu, S. et al. Poly (vinyl alcohol) hydrogels with broad-range tunable mechanical properties via the hofmeister effect. *Adv. Mater.* **33**, 2007829 (2021).
12. Hassani, F. A. et al. Smart materials for smart healthcare–moving from sensors and actuators to self-sustained nanoenergy nanosystems. *Smart Mater. Med.* **1**, 92–124 (2020).
13. Liu, K., Tian, Y. & Jiang, L. Bio-inspired superoleophobic and smart materials: design, fabrication, and application. *Prog. Mater. Sci.* **58**, 503–564 (2013).
14. Xu, S. et al. Soft microfluidic assemblies of sensors, circuits, and radios for the skin. *Science* **344**, 70–74 (2014).
15. Soto, F. et al. Smart materials for microrobots. *Chem. Rev.* **122**, 5365–5403 (2021).
16. Liebchen, B. & Levis, D. Collective behavior of chiral active matter: pattern formation and enhanced flocking. *Phys. Rev. Lett.* **119**, 058002 (2017).
17. Bär, M., Großmann, R., Heidenreich, S. & Peruani, F. Self-propelled rods: Insights and perspectives for active matter. *Annu. Rev. Condens. Matter Phys.* **11**, 441–466 (2020).
18. Bowick, M. J., Fakhri, N., Marchetti, M. C. & Ramaswamy, S. Symmetry, thermodynamics, and topology in active matter. *Phys. Rev. X* **12**, 010501 (2022).
19. Levine, H., Goldman, D.I. Physics of smart active matter: integrating active matter and control to gain insights into living systems. *Soft Matter* **19**, 4204-4207 (2023).
20. Savoie, W., Tuazon, H., Tiwari, I., Bhamla, M. S. & Goldman, D. I. Amorphous entangled active matter. *Soft Matter* **19**, 1952–1965 (2023).
21. Vernerey, F. et al. Biological active matter aggregates: inspiration for smart colloidal materials. *Adv. Colloid Interface Sci.* **263**, 38–51 (2019).
22. Pishvar, M. & Harne, R. L. Foundations for soft, smart matter by active mechanical metamaterials. *Adv. Sci.* **7**, 2001384 (2020).
23. Glotzer, S. C. & Solomon, M. J. Anisotropy of building blocks and their assembly into complex structures. *Nat. Mater.* **6**, 557–562 (2007).
24. Xu, S. et al. Assembly of micro/nanomaterials into complex, three-dimensional architectures by compressive buckling. *Science* **347**, 154–159 (2015).
25. Li, Z., Fan, Q. & Yin, Y. Colloidal self-assembly approaches to smart nanostructured materials. *Chem. Rev.* **122**, 4976–5067 (2021).
26. Lee, J.-Y., An, J. & Chua, C. K. Fundamentals and applications of 3d printing for novel materials. *Appl. Mater. Today* **7**, 120–133 (2017).
27. Miszta, K. et al. Hierarchical self-assembly of suspended branched colloidal nanocrystals into superlattice structures. *Nat. Mater.* **10**, 872–876 (2011).
28. Damasceno, P. F., Engel, M. & Glotzer, S. C. Predictive self-assembly of polyhedra into complex structures. *Science* **337**, 453–457 (2012).
29. Mao, X., Chen, Q. & Granick, S. Entropy favours open colloidal lattices. *Nat. Mater.* **12**, 217–222 (2013).
30. English, M. A. et al. Programmable crispr-responsive smart materials. *Science* **365**, 780–785 (2019).
31. Kumar, R. et al. Revisiting fluorescent calixarenes: from molecular sensors to smart materials. *Chem. Rev.* **119**, 9657–9721 (2019).
32. Rubenstein, M., Cornejo, A. & Nagpal, R. Programmable self-assembly in a thousand-robot swarm. *Science* **345**, 795–799 (2014).
33. Xie, H. et al. Reconfigurable magnetic microrobot swarm: multimode transformation, locomotion, and manipulation. *Sci. Robot.* **4**, 8006 (2019).
34. Wang, G. et al. Emergent field-driven robot swarm states. *Phys. Rev. Lett.* **126**, 108002 (2021).
35. Yao, T. et al. Nematic colloidal micro-robots as physically intelligent systems. *Adv. Funct. Mater.* **32**, 2205546 (2022).
36. Wang, X. et al. Colloidal tubular microrobots for cargo transport and compression. *Proc. Natl Acad. Sci. USA* **120**, 2304685120 (2023).
37. Berlinger, F., Gauci, M. & Nagpal, R. Implicit coordination for 3d underwater collective behaviors in a fish-inspired robot swarm. *Sci. Robot.* **6**, 8668 (2021).
38. Yim, M. et al. Modular self-reconfigurable robot systems [grand challenges of robotics]. *IEEE Robot. Autom. Mag.* **14**, 43–52 (2007).
39. Li, S. et al. Particle robotics based on statistical mechanics of loosely coupled components. *Nature* **567**, 361–365 (2019).
40. Saintyves, B., Spenko, M. & Jaeger, H. M. A self-organizing robotic aggregate using solid and liquid-like collective states. *Sci. Robot.* **9**, 4130 (2024).
41. Ozkan-Aydin, Y., Goldman, D. I. & Bhamla, M. S. Collective dynamics in entangled worm and robot blobs. *Proc. Natl Acad. Sci. USA* **118**, 2010542118 (2021).
42. Li, S. et al. Programming active cohesive granular matter with mechanically induced phase changes. *Sci. Adv.* **7**, 8494 (2021).
43. Salman, M., Garzón Ramos, D., Hasselmann, K. & Birattari, M. Phormica: photochromic pheromone release and detection system for stigmergic coordination in robot swarms. *Front. Robot. AI* **7**, 591402 (2020).
44. Salman, M., Garzón Ramos, D. & Birattari, M. Automatic design of stigmergy-based behaviours for robot swarms. *Commun. Eng.* **3**, 30 (2024).
45. Schranz, M., Umlauft, M., Sende, M., Elmenreich, W. Swarm robotic behaviors and current applications. *Front. Robot. AI* **7**, 36 (2020).
46. Dorigo, M., Theraulaz, G. & Trianni, V. Swarm robotics: past, present, and future [point of view]. *Proc. IEEE* **109**, 1152–1165 (2021).
47. Aguilar, J. et al. A review on locomotion robophysics: the study of movement at the intersection of robotics, soft matter and dynamical systems. *Rep. Prog. Phys.* **79**, 110001 (2016).
48. Slavkov, I. et al. Morphogenesis in robot swarms. *Sci. Robot.* **3**, 9178 (2018).
49. Wang, G. et al. Robots as models of evolving systems. *Proc. Natl Acad. Sci. USA* **119**, 2120019119 (2022).
50. Zhang, H. et al. Dual-responsive biohybrid neutrobots for active target delivery. *Sci. Robot.* **6**, 9519 (2021).

51. Jin, D. et al. Swarming self-adhesive microgels enabled aneurysm on-demand embolization in physiological blood flow. *Sci. Adv.* **9**, 9278 (2023).
52. McEvoy, M. A. & Correll, N. Materials that couple sensing, actuation, computation, and communication. *Science* **347**, 1261689 (2015).
53. Kaspar, C., Ravoo, B., Wiel, W. G., Wegner, S. & Pernice, W. The rise of intelligent matter. *Nature* **594**, 345–355 (2021).
54. Savoie, W. et al. A robot made of robots: emergent transport and control of a smarticle ensemble. *Sci. Robot.* **4**, 4316 (2019).
55. Al-Shehri, H., Horozov, T. S. & Paunov, V. N. Preparation and attachment of liquid-infused porous supra-particles to liquid interfaces. *Soft Matter* **12**, 8375–8387 (2016).
56. Juárez, J. J. & Bevan, M. A. Feedback controlled colloidal self-assembly. *Adv. Funct. Mater.* **22**, 3833–3839 (2012).
57. Lavergne, F. A., Wendehenne, H., Bäuerle, T. & Bechinger, C. Group formation and cohesion of active particles with visual perception–dependent motility. *Science* **364**, 70–74 (2019).
58. Scholz, C., Engel, M. & Pöschel, T. Rotating robots move collectively and self-organize. *Nat. Commun.* **9**, 931 (2018).
59. Yang, Q. et al. Topologically protected transport of cargo in a chiral active fluid aided by odd-viscosity-enhanced depletion interactions. *Phys. Rev. Lett.* **126**, 198001 (2021).
60. Kokot, G. et al. Active turbulence in a gas of self-assembled spinners. *Proc. Natl Acad. Sci. USA* **114**, 12870–12875 (2017).
61. Liao, G.-J. & Klapp, S. H. Emergent vortices and phase separation in systems of chiral active particles with dipolar interactions. *Soft Matter* **17**, 6833–6847 (2021).
62. Petroff, A. P., Wu, X.-L. & Libchaber, A. Fast-moving bacteria self-organize into active two-dimensional crystals of rotating cells. *Phys. Rev. Lett.* **114**, 158102 (2015).
63. Tan, T. H. et al. Odd dynamics of living chiral crystals. *Nature* **607**, 287–293 (2022).
64. Porter, D.A., Easterling, K.E., Sherif, M.Y. *Phase Transformations in Metals and Alloys* (CRC Press, 2021)
65. Sun, J., Guan, Q., Liu, Y. & Leng, J. Morphing aircraft based on smart materials and structures: a state-of-the-art review. *J. Intell. Mater. Syst. Struct.* **27**, 2289–2312 (2016).
66. Efrati, E. & Irvine, W. T. Orientation-dependent handedness and chiral design. *Phys. Rev. X* **4**, 011003 (2014).
67. Dietler, G., Kusner, R., Kusner, W., Rawdon, E., Szymczak, P. Chirality for crooked curves. Preprint at arXiv:2004.10338 (2020)
68. Werfel, J., Petersen, K. & Nagpal, R. Designing collective behavior in a termite-inspired robot construction team. *Science* **343**, 754–758 (2014).
69. Romanishin, J.W., Gilpin, K., Claici, S., Rus, D. 3d m-blocks: Self-reconfiguring robots capable of locomotion via pivoting in three dimensions. In *2015 IEEE International Conference on Robotics and Automation (ICRA)* 1925–1932 (IEEE, 2015).
70. Li, H., Wei, H., Xiao, J. & Wang, T. Co-evolution framework of swarm self-assembly robots. *Neurocomputing* **148**, 112–121 (2015).
71. Wang, J. et al. Robo-matter towards reconfigurable multifunctional smart materials. *Zenodo* https://doi.org/10.5281/zenodo.13837240 (2024).

Acknowledgements

This research was supported by the National Natural Science Foundation of China (Grant Nos. 12174041, T2350007 to L.L. and 12090052 to J.S.), China Postdoctoral Science Foundation (CPSF, Grant No. 2022M723118 to G.W.), and the seed grants from the Wenzhou Institute, University of Chinese Academy of Sciences (Grant No. WIUCASQD2021002 to L.L.). Y.J. and Jin W. did not have any financial support for this work.

Author contributions

L.L., Y.J., Jing W., and G.W. conceived and designed the research. Jing W., G.W., and H.C. are joint first authors. Jing W. designed and performed experiments and simulations and analysed data. G.W. designed and prepared the Magbots and the experimental system and designed experiments. H.C. prepared the experimental system, designed and performed experiments, and analysed data. Y.L., P.W., and D.Y. prepared the Magbots and the experimental system and performed experiments. X.M. performed experiments and analysed data. X.X., Z.C., B.J., and M.Y. performed simulations and analysed data. J.S., F.Y., and Jin W. analysed data. L.L. and Y.J. designed experiments and simulations and supervised research. All authors discussed the results and co-wrote the paper.

Competing interests

The authors declare no competing interests.

Additional information

Supplementary information The online version contains supplementary material available at https://doi.org/10.1038/s41467-024-53123-6.

Correspondence and requests for materials should be addressed to Yang Jiao or Liyu Liu.

Peer review information *Nature Communications* thanks Hui Xie, Razanne Abu-Aisheh, and the other, anonymous, reviewer(s) for their contribution to the peer review of this work. A peer review file is available.

[1]Wenzhou Institute, University of Chinese Academy of Sciences, Wenzhou 325001 Zhejiang, China. [2]School of Physical Sciences, University of Chinese Academy of Sciences, Beijing 100049, China. [3]College of Physics, Chongqing University, Chongqing 401331, China. [4]College of Chemical and Biological Engineering, Zhejiang University, Hangzhou 310058 Zhejiang, China. [5]Institute of Biomechanics and Applications, Department of Engineering Mechanics, Zhejiang University, Hangzhou 310027 Zhejiang, China. [6]Beijing National Laboratory for Condensed Matter Physics and Laboratory of Soft Matter Physics, Institute of Physics, Chinese Academy of Sciences, Beijing 100190, China. [7]Department of Chemistry, Physics and Applied Mathematics, State University of New York at Stony Brook, New York 11794-3400 NY, USA. [8]Materials Science and Engineering, Arizona State University, Tempe 85287 AZ, USA. [9]Department of Physics, Arizona State University, Tempe 85287 AZ, USA. [10]Present address: Beijing National Laboratory for Condensed Matter Physics and Laboratory of Soft Matter Physics, Institute of Physics, Chinese Academy of Sciences, Beijing 100190, China. ✉e-mail: yang.jiao.2@asu.edu; lyliu@cqu.edu.cn